Fear Conditioning Potentiates the Hippocampal CA1 Commissural Pathway In vivo and Increases Awake Phase Sleep

Manivannan Subramaniyan, Sumithrra Manivannan,
Vikas Chelur, Theodoros Tsetsenis, Evan Jiang and John A. Dani*

Department of Neuroscience, Mahoney Institute for Neurosciences,
Perelman School for Medicine, Philadelphia, PA 19104 USA

Running Title: Fear Conditioning Potentiates the Commissural Pathway

* Address all correspondences to John A. Dani, Department of Neuroscience, University of Pennsylvania, Philadelphia, PA 19104; Email: johndani@pennmedicine.upenn.edu

Abstract

The hippocampus is essential for spatial learning and memory. To assess learning we used contextual fear conditioning (cFC), where animals learn to associate a place with aversive events such as foot-shocks. Candidate memory mechanisms for cFC are long-term potentiation and long-term depression, but there is little direct evidence of those mechanisms operating in the hippocampus in vivo following cFC. Also, little is known about the behavioral state changes induced by cFC. To address these shortcomings, we used motion tracking and recorded local field potentials in freely behaving mice by placing a stimulating electrode in the left dorsal CA1 region and positioning recording electrodes in the right dorsal CA1 region. Synaptic strength in the commissural pathway was monitored by measuring field excitatory postsynaptic potentials (fEPSPs) before and after cFC. After cFC, the commissural pathway's synaptic strength was potentiated. Although recordings were conducted during the wake phase of the light/dark cycle, the mice slept more in the post-conditioning period than in the pre-conditioning period. Relative to awake periods, in non-rapid eye movement (NREM) sleep the fEPSPs were larger in both pre- and post-conditioning periods. Therefore, to avoid sleep-related fEPSP changes confounding the effects of cFC learning, we accounted for the effects of sleep and still found long-term potentiation of the commissural pathway, but no significant long-term depression. Synaptic strength changes were not found in the no-shock, control group that simply explored the fear-conditioning chamber, indicating that exploration of the novel place did not produce the measurable effects caused by cFC. These results show that following cFC, the CA1 commissural pathway is potentiated, likely contributing to the functional integration of the left and right hippocampi in fear memory consolidation. In addition, the cFC paradigm produces significant changes in an animal's behavioral state, which are observable as proximal changes in sleep patterns.

Key words: fear conditioning, learning and memory, non-rapid eye movement sleep, in vivo plasticity, behavioral state, long-term potentiation

Introduction

Learning and memory are vital for the survival of animals, so disorders affecting these systems are debilitating. Contextual fear- conditioning (cFC) is an associative learning paradigm and a commonly used model of clinical anxiety disorders (Maren, Phan, & Liberzon, 2013; Shin & Liberzon, 2010). In this task, animals learn within a single 5-10 minute trial to associate a distinct place with foot-shocks. Thus, this assay enables the observation of neural circuit changes across distinct learning phases (e.g. memory acquisition, consolidation, and recall) on a relatively brief timescale. Learning in this task requires the hippocampus (Maren et al., 2013), whose well-defined synaptic pathways are amenable to experimental manipulations. By leveraging the tractability of hippocampal pathways and the cFC behavioral assay, we examined real-time neural circuit changes associated with fear memories. Ideally those pathways may provide targets for the ongoing development of treatments aimed at relieving stress-related memory disorders.

The mechanisms of associative fear memory are complex and involve molecular to systems-level changes in the brain, and fully understanding these mechanisms will require integrating information from various levels of neural function (Sporns, 2011). Most studies to date have focused on either the systems-level or the molecular/structural level. At the systems-level, recent studies have focused on associative fear memory-induced changes in network activity, inter-regional coupling, neuronal oscillations and synchrony, engram and place field formation (Girardeau, Inema, & Buzsáki, 2017; Karunakaran et al., 2016; Lesting et al., 2013; Likhtik, Stujenske, A Topiwala, Harris, & Gordon, 2013; Moita, Rosis, Zhou, LeDoux, & Blair, 2004; Narayanan, Seidenbecher, Sangha, Stork, & Pape, 2007; Ognjanovski, Maruyama, Lashner, Zochowski, & Aton, 2014; Ognjanovski et al., 2017; Pape, Narayanan, Smid, Stork, & Seidenbecher, 2005; Popa, Duvarci, Popescu, Lena, & Pare, 2010; Seidenbecher, Laxmi, Stork, & Pape, 2003; Tonegawa, Liu, Ramirez, & Redondo, 2015; Wang et al., 2012). At the molecular and structural level, studies have focused on changes in intracellular signaling, receptor and ion channel function and neuronal morphology that are associated with fear memory formation (Buffington, Huang, & Costa-Mattioli, 2014; Johansen, Cain, Ostroff, & LeDoux, 2011; Nicoll, 2017; Penn et al., 2017). These studies imply that these molecular/structural changes should lead to systems-level changes, and the link between these levels should be circuit-level changes, which manifest as changes in synaptic strength. While a handful of seminal studies have shown that learning-related changes in synaptic strength do occur in vivo in some aversive learning paradigms (Broussard et al., 2016; Gruart, Munoz, & Delgado-Garcia, 2006; Whitlock, Heynen, Shuler, & Bear, 2006), this crucial link has not been established for cFC.

The hippocampal commissural pathways are highly conserved during evolution (Suárez, Gobius, & Richards, 2014) and, they strongly interconnect the subregions of the left and right hippocampi (Laurberg, 1979; Swanson, Wyss, & Cowan, 1978). However, the functions of these connections are only beginning to be unraveled (Phelps, Hirst, & Gazzaniga, 1991; Schimanski, Wahlsten, & Nguyen, 2002; Zhou et al., 2017). Although in vivo LTP can be artificially induced in these pathways (Bliss, Lancaster, & Wheal, 1983; Martin, Shires, & da Silva, 2019; Stäubli & Scafidi, 1999), it is unknown if plasticity occurs in vivo in these pathways in association with cFC. Moreover, unlike artificially induced plasticity, learning-related changes are widely distributed (Eichenbaum, 2016), making their detection harder at the circuit level. Hence, although fear conditioning-related plasticity likely occurs in the commissural pathways, it is unknown if it will be detectable in vivo. Also unknown is the plasticity's temporal profile, which may be very different from that resulting from artificial plasticity induction owing to potential changes in the animal's behavioral states accompanying learning. Hence, to characterize how the commissural pathway's strength changes in association with behavioral learning, we periodically monitored the synaptic strength of the dorsal CA1 commissural pathway before and immediately after the cFC task. One impediment to assessing learning-related synaptic changes in this pathway is that, behavioral states such as wakeful voluntary motion, still alertness, REM sleep, and NREM or slow wave sleep, are also

known to influence excitability and synaptic transmission in the hippocampus (Buzsaki, Grastyan, Czopf, Kellenyi, & Prohaska, 1981; Green, McNaughton, & Barnes, 1990; Grosmark, Mizuseki, Pastalkova, Diba, & Buzsáki, 2012; Hulse, Lubenov, & Siapas, 2017; Segal, 1978; Winson & Abzug, 1977, 1978a, 1978b). To isolate learning-related effects from potential behavioral state-related effects on synaptic plasticity measurements, we monitored the animal's gross behavioral states using motion tracking and power spectral analysis of hippocampal recordings.

Our analyses showed that following cFC, behavioral states changed: mice slept more after the cFC although they were in the wake phase of their light/dark cycle. During the NREM part of these sleep periods, the fEPSPs were larger in amplitude, and we accounted for this potential confound when measuring the cFC-induced synaptic changes. While we did not find evidence for long-term depression, our results showed that the dorsal CA1 commissural pathway undergoes significant in vivo long-term potentiation in real-time following cFC.

Results

To determine whether long-lasting synaptic changes occur in the hippocampal synapses due to associative learning, we measured synaptic strength in the commissural pathway of the dorsal CA1 region in freely moving mice (Fig. 1A). We placed a stimulating electrode in the left CA1 and positioned one or more recording electrodes in the right CA1 (Fig. 1B). With this configuration, the stimulation response in the right CA1 arises predominantly from activation of direct commissural projections from the left CA1 (Zhou et al., 2017). Synaptic strength was quantified by periodically measuring the slope of the population field EPSP (fEPSP) arising from brief electrical stimulation (Fig. 1C-D). All experiments were done during the awake (dark) phase of the animals' light/dark cycle (Fig. 1E). During recordings, mice remained undisturbed in their home cage that was placed inside a sound-attenuating recording chamber. After a 2h baseline measurement, mice were removed from their home cage and subjected to cFC (n = 24, Fig. 1E). To examine the conditioning-related neural changes immediately following fear conditioning, synaptic strength was measured again for another 3h. After these recordings, fear memory was tested 24h post-conditioning in one group of mice (n = 12) and 1-week post-conditioning in a second group of mice (n = 12). Both groups showed significant memory retention suggesting that the conditioning protocol effectively induced long-lasting memory ($p < 10^{-5}$ for both groups, t-test; % freezing after 24h, 37 ± 4%, mean ± 1SE; after 1-week, 49 ± 5%; no significant difference between 24h and 1 week, p = 0.058, t-test).

Stimulation and recording sites were restricted to the dorsal CA1 region (Fig. 2A). To quantify fear conditioning-related synaptic strength changes, we first normalized all fEPSP slopes of a given electrode to the mean fEPSP slope of the baseline period of the same electrode. Figure 2B shows the normalized fEPSP slopes of all the electrodes. There were multiple recording electrodes (2-7) in most mice. Hence, one approach to compute the overall learning-related effects could be to average the data across all the electrodes within each mouse before pooling across mice. As reported previously (Whitlock et al., 2006), however, we expected that different electrodes within a mouse might show either potentiation, depression, or no change in synaptic strength. Consequently, averaging the changes across electrodes could cancel out synaptic strength changes. Therefore, to identify learning effects, we examined potentiation and depression separately. For potentiation, we chose one electrode from each mouse as follows. In the subset of mice (18/24) that had multiple electrodes, for each mouse, we chose a single electrode that had the largest potentiation. To this set of selected electrodes, we added the electrodes from the rest of the mice (6/24) that had a single electrode per mouse. Note that although depression or no change may be found in some of the electrodes of the single-electrode mice, to get a conservative estimate of potentiation, we decided to combine all the single electrode cases with the data from the most-potentiated electrodes from mice that had multiple electrodes. This process will lead only to an underestimation of measureable synaptic potentiation.

Following fear conditioning, many electrodes showed a small potentiation, some showed no change, and depression was rare (Fig. 2B). Data from the most-potentiated electrode of the implanted set are shown for an example mouse in Figure 2C where a sustained increase in synaptic strength can be seen. Data from all of the most-potentiated electrodes are shown in Figure 2D with warmer red colors indicating potentiation. On average, the post-conditioning period showed substantial potentiation compared to baseline (Fig. 2E). To assess the statistical significance of the results, we used a linear mixed model (LMM) approach, treating the sequence of fEPSP slopes as an interrupted time series (Wagner, Soumerai, Zhang, & Ross-Degnan, 2002) where the post-conditioning fEPSP slopes result from fear conditioning "interrupting" the sequence of baseline fEPSP slopes (see Methods). The analysis showed that the baseline was stable for 2h, i.e., there was no significant change of fEPSP slopes over time ($F(1, 3943.3) = 0.058$, $p = 0.81$, LMM). Following learning, there was a significant increase in the fEPSP slopes ($F(1, 4152.8) = 7.63$, $p = 0.006$, LMM). In the post-conditioning period, the synaptic strength also grew larger with time ($F(1, 3765.7) = 6.8$, $p = 0.009$, LMM). These data suggest that after fear conditioning, a subset of commissural synapses undergo long-term potentiation in the dorsal CA1 region.

In addition to learning, an animal's behavioral state is also known to modulate hippocampal synaptic transmission. Associative and commissural synaptic inputs from CA3 have a stronger excitatory effect on CA1 fEPSP during NREM sleep, compared to the awake state or REM sleep (Segal, 1978; Winson & Abzug, 1977, 1978a, 1978b). Although all our experiments were done during the awake phase of the light/dark cycle, we still considered the possibility that after fear conditioning, the mice may sleep which could produce increased fEPSPs that would inflate the appearance of synaptic potentiation. In fact, such NREM sleep-mediated enhancement of synaptic strength could potentially explain the noticeable increase of fEPSP slopes during the final 30-minute period of post-conditioning recording (seen in Fig. 3A indicated by the arrow). Others have shown that NREM sleep can be detected in the field recordings by a drop in theta band (5-11Hz) power and an increase in delta band (1-4Hz) power (Grosmark et al., 2012; Mizuseki, Diba, Pastalkova, & Buzsáki, 2011; Rothschild, Eban, & Frank, 2017; Sirota et al., 2008); that is indeed the case during the 30-minute time period (Fig. 3B). Following previously published guidelines (Grosmark et al., 2012), we identified NREM state as the period when the animal was not moving and there was a sustained decrease in the theta/delta power ratio (Fig. 3C) compared to when the animal was moving (Fig. 3D). During awake periods, the motion level was variable, arising from multiple awake states (Hulse et al., 2017), and we simply grouped them into one "awake" behavioral state. We then averaged the waveform of all the stimulated fEPSPs within awake and NREM states. In the awake state, the average stimulation response after training was higher than that of baseline (Fig. 3E). Interestingly, during post-conditioning NREM periods, this effect was further enhanced, possibly reflecting participation of NREM in memory-consolidation mechanisms. To explore this further, we examined the NREM effect across all the mice we tested.

To identify sleep states, we computed the theta/delta ratio and the motion index, both normalized to baseline. Note that, the theta/delta ratio modulation was similar across all the electrodes of a multi-electrode set within a given mouse. Segments with a sustained decrease in the theta/delta ratio (Fig. 4A, cold blue colors) and corresponding immobility (Fig. 4B, cold blue colors) were labeled as NREM states. REM states were identified by an increase in the theta/delta ratio that corresponded with animal immobility. These two states of sleep were grouped into a single "sleep" state (Fig. 4C). Visual inspection of Figure 4C shows that only a few animals slept briefly during baseline (median 0%, min 0%, max 20%, Fig. 4D). However, a majority of animals slept intermittently after fear conditioning (median 16%, min 0%, max 55%), resulting in a significantly higher proportion of time spent sleeping in the post-conditioning period ($p = 1.9 \times 10^{-6}$, $n = 24$, sign test). As seen in the example mouse data (Fig. 3), the averaged slope of the NREM epochs (duration of at least 5 min) was higher compared to that of the awake state for each mouse ($n = 19$, Fig. 4E). On average, the NREM state slopes were 1.3 ± 0.01 (mean ± 1SE) times higher

than those of awake state (Fig. 4F, $p = 2.7 \times 10^{-15}$, n = 19, ratio t-test). Of note, the NREM-mediated enhancement of fEPSP slopes was also evident during the baseline in three mice that slept at least 5 min (Fig. 4E-F, filled magenta circles). This suggests that NREM state can boost the fEPSP slopes irrespective of learning, which is in accordance with previous studies (Winson & Abzug, 1977, 1978a, 1978b) that also found similar enhanced synaptic responses during NREM state in non-learning conditions. Evidence implicates sleep as an integral component of memory consolidation (Abel, Havekes, Saletin, & Walker, 2013; Klinzing, Niethard, & Born, 2019; Walker & Stickgold, 2006). Hence, the sleep periods following cFC may serve important functions related to memory consolidation. However, for a conservative estimate of the synaptic potentiation that might contribute to learning, we set out to remove the slope data corresponding to sleep segments that would exaggerate the synaptic potentiation.

Starting with the original complete dataset (Fig. 2B), we removed the fEPSP slopes corresponding to the sleep segments from baseline and post-conditioning periods and, then, normalized all slopes to the baseline. As described for Figure 2, a single electrode was then chosen from each mouse to form the most-potentiated electrode set. Figure 4G shows the across-mouse average of fEPSP slopes after removing the sleep segments. Data from the same electrodes are shown in Figures 2E and 4G to aid in comparison of the synaptic potentiation effect with (Fig. 2E) and without (Fig. 4G) sleep. Interestingly, even after removing the NREM-mediated enhancement of synaptic transmission, the fEPSP slopes were still significantly increased in the post-conditioning period ($F(1, 1626.8) = 11.9$, $p = 0.001$, LMM). Within the baseline and post-conditioning period, fEPSP slopes did not change over time (baseline: $F(1, 1568.4) = 0.21$, $p = 0.645$; post-conditioning period: $F(1, 1532.7) = 0.007$, $p = 0.936$, LMM), indicating respectively that the baseline remained stable and that the synaptic potentiation effect persisted throughout the post-conditioning period. These results suggest that the fear conditioning resulted in long-term potentiation of the commissural pathway in a subset of locations in the dorsal CA1 region and that this effect cannot be explained by the sleep state.

Long-term depression has also been proposed to participate in learning and memory (Bear, 1996; Kemp & Manahan-Vaughan, 2004; Malenka & Bear, 2004). To test whether cFC resulted in any significant decrease in the average fEPSP slopes, we first removed slope data corresponding to the sleep segments and normalized the slopes to baseline as we did in Fig. 4G. Then, from each mouse that had multiple electrodes (n = 18 mice), the least-potentiated electrode was selected. Unlike our analysis of potentiation, mice with single electrodes (n = 6) were excluded as any potentiation in some of them would mask any possible depression effects. Following cFC, relative to baseline, there was no significant change in fEPSP slopes (Fig. 4H)($F(1, 1227.1) = 0.55$, $p = 0.458$, LMM). Within the baseline and post-conditioning period, fEPSP slopes did not change over time (baseline: $F(1, 1180.5) = 0.19$, $p = 0.663$; post-conditioning period: $F(1, 1150.2) = 0.128$, $p = 0.720$, LMM)), indicating respectively that the baseline remained stable and that the synaptic strength remained unchanged throughout the post-conditioning period. These results show that fear conditioning did not result in measureable (with our protocols) long-term depression of the commissural synapses onto the dorsal CA1 region.

We did not habituate the animals to the fear conditioning chamber, and the mice had not been used in any previous behavioral tasks. As a result, our fear conditioning task inherently included exploration of a novel place (i.e., the conditioning chamber), which by itself may have contributed to the synaptic potentiation we observed. To address this issue, we tested synaptic strength before and after a sham-fear conditioning procedure (Fig. 5A-B) where the animals explored the conditioning chamber but no foot-shocks were given. The sleep patterns (Fig. 5C) indicated that most animals stayed awake throughout the duration of the recording (baseline: median, 0%, min, 0%, max, 5%; post-conditioning: median, 0%, min, 0%, max, 12%) with no significant change in the sleep after the sham-fear conditioning procedure compared to baseline ($p = 0.375$, n = 12, signtest). This sleep pattern is in contrast to that of

the shocked group, which, compared to the sham-trained group, slept more during post-conditioning relative to baseline ($p = 2.13 \times 10^{-4}$, n = 24, 12, one-tailed ranksum test on post-pre difference in sleep %). However, similar to the shocked group, when the sham-trained animals went to NREM sleep, the fEPSP responses were higher relative to those of awake state (for the 3 mice with at least 5 min of NREM sleep, fEPSP slope NREM/awake ratio: 1.53, 1.28 and 1.46). Hence, following the same procedure used for the fear-conditioned animals (Fig. 4G), we chose the most potentiated electrodes after removing the fEPSP slope data that corresponded to the sleep segments. The across-mouse average (Fig. 5D) shows that there was no significant change in synaptic strength in the post-sham training session relative to baseline ($F(1, 894.1) = 1.1$, $p = 0.295$, LMM). Within the baseline and post-conditioning period, fEPSP slopes did not change over time (baseline: $F(1, 867.1) = 1.26$, $p = 0.262$; post-sham training periods: $F(1, 839.9) = 3.479$, $p = 0.063$, LMM), indicating respectively that the baseline remained stable and that the synaptic strength remained unchanged throughout the post-sham training period. These results suggest that exploration of a novel place – the fear conditioning chamber – was not sufficient to result in significant measureable changes in synaptic strength. Furthermore, relative to the sham-conditioning control, fear-conditioned animals showed a significant potentiation in the post-conditioning session (significant pre-post x shock condition interaction, $F(1, 2371.5) = 7.11$, $p = 0.008$, LMM). Together, these results clearly demonstrate that fear conditioning potentiates the commissural pathway of the dorsal CA1, and that this potentiation cannot be explained by sleep state or exploration of a novel environment.

Discussion

Contextual fear-conditioning has been used for decades as a model for associative fear learning. Although numerous studies have observed cFC-related changes at the cellular, synaptic, and molecular level in the hippocampus (Buffington et al., 2014; Johansen et al., 2011; Nicoll, 2017; Sacchetti et al., 2001), real-time in vivo synaptic plasticity has not been examined. Our data demonstrate that a specific circuit of the hippocampus, the dorsal CA1 commissural pathway, undergoes long-term potentiation but not long-term depression in vivo in association with the fear conditioning task. Our data also show that sleep is more common after cFC and that the size of the fEPSP responses are bigger during NREM sleep than during the awake state, emphasizing the importance of taking an animal's behavioral state into account when measuring learning-related synaptic changes.

In spite of the numerous commissural fibers connecting subregions of the two hippocampi in rodents (Laurberg, 1979; Swanson et al., 1978), the function of this pathway is not well characterized. One recent study in rats suggests that the dorsal hippocampal CA1 to CA1 commissural pathway is involved in a rapid form (< 24h) of fear generalization (Zhou et al., 2017) that is distinct from previously studied fear generalization that develops over many days (Cullen, Gilman, Winiecki, Riccio, & Jasnow, 2015; dos Santos Corrêa et al., 2019; Pedraza et al., 2016; B. J. Wiltgen & Silva, 2007; Brian J. Wiltgen et al., 2010). However, the rapid generalization that was observed (Zhou et al., 2017) depended on pre-exposure to two different contexts (conditioning and non-conditioning) the day before the conditioning. In this paradigm, contrary to our results, the authors show no plasticity in the commissural pathway following the conditioning. Given that our experimental paradigm is different from that used by Zhou et al. (Zhou et al., 2017), the plasticity we observed immediately after conditioning is unlikely to be related to the rapid fear-generalization they describe. Under our experimental conditions, observed results suggest that the commissural pathway may be involved in a specific component of the learning task. An important next step would be to test if the potentiation we observed is related to learning of the conditioning context or related to linking the context with the aversive events occurring in that context. Because exposure to the conditioning chamber (without shocks) did not result in synaptic potentiation, learning the context or place is not sufficient to produce the commissural potentiation, suggesting the pathway may contribute to linking the aversive event to the context.

It should be noted that the LTP effect observed in Figure 2E appears to grow over time. However, when the sleep-related behavioral state is accounted for (Fig. 4G), the in vivo LTP remained stable over time rather than growing or declining. These observations suggest the importance of taking behavioral state into account when assessing the dynamics of in vivo LTP. In this regard, the use of linear mixed model approach to statistically analyze the sleep-interrupted data is helpful because it can handle missing data and quantitatively assess linear trends.

The magnitude of the LTP in the dorsal CA1 we observed (i.e., a 10% change) is smaller than experimentally stimulus-induced in vivo LTP, which typically produces a > 50-100% change (Martin et al., 2019). The magnitude we observed is comparable to the in vivo plasticity seen in studies of inhibitory avoidance (Broussard et al., 2016; Whitlock et al., 2006) and eyeblink conditioning (Gruart et al., 2006). The smaller in vivo LTP likely results from a low signal-to-noise ratio. That is, plastic changes may happen only at a subset of synapses that are distributed widely in the hippocampus. Given that our fEPSP measurement sums the effect of a large number of synapses most of which are likely unmodified, the contribution of the smaller number of modified synapses in any given recording location gets diluted within the overall average, giving rise to smaller LTP measurements.

Although all our experiments were done during the dark (i.e., awake) phase of the light/dark cycle, we found that the fear-conditioned mice spent more time in intermittent sleep compared to the sham-conditioned group. To the best of our knowledge, this has not been reported before, although many studies (Ambrosini et al., 1993; Bramham, Maho, & Laroche, 1994; Datta, 2000; Hellman & Abel, 2007; Mavanji, Siwek, Patterson, Spoley, & Datta, 2003; Pawlyk, Morrison, Ross, & Brennan, 2008; Larry D. Sanford, Fang, & Tang, 2003; L. D. Sanford, Tang, Ross, & Morrison, 2003; Smith, Young, & Young, 1980; Wellman, Yang, Tang, & Sanford, 2008) have found changes in light phase sleep architecture in rodents that were subjected to shock training during the light phase or briefly before the light onset. The mechanisms of the conditioning-induced awake-phase (i.e., dark-phase) sleep are unclear. Interestingly, the sleep studies that were conducted during the dark phase (Bonnet, Léger, Baubet, Debilly, & Cespuglio, 1997; del C. Gonzalez, Debilly, Valatx, & Jouvet, 1995; Koehl, Bouyer, Darnaudéry, Le Moal, & Mayo, 2002; Rampin, Cespuglio, Chastrette, & Jouvet, 1991), consistently found that rats that were subjected to brief (~1h) immobilization stress during the dark phase, slept more in the dark phase compared to non-stressed rats. Thus, foot-shock stress, though different from immobilization stress, can be speculated to contribute to the increased dark-phase sleep following fear-conditioning. Irrespective of the mechanisms behind this increased sleep, sleep disruption for 5h immediately following fear-conditioning leads to memory impairment (Graves, Heller, Pack, & Abel, 2003). Conversely, inducing sleep immediately after training facilitates memory consolidation (Donlea, Thimgan, Suzuki, Gottschalk, & Shaw, 2011). During NREM sleep, sharp-wave ripples - high frequency oscillations of approximately 200 Hz in the field potential arising from synchronous rhythmic firing of hippocampal neurons - are abundant, and have been implicated in learning and memory (G. Buzsáki, 2015; Joo & Frank, 2018; Olafsdottir, Bush, & Barry, 2018). Ripple disruption during the NREM sleep and rest that follow immediately after spatial learning, impairs learning (Girardeau, Benchenane, Wiener, Buzsáki, & Zugaro, 2009). Together, these studies suggest that the increased sleep we observed likely serves an important function in memory consolidation.

Although the effect of the animal's brain state on subthreshold activity, spiking, and network activity in the hippocampus have been extensively studied (György Buzsáki, Lai-Wo S, & Vanderwolf, 1983; Chrobak & Buzsáki, 1996; Hulse et al., 2017; Jarosiewicz, McNaughton, & Skaggs, 2002; Kay et al., 2016; O'Keefe, 1976; Wilson & McNaughton, 1994), only a handful of rat studies have examined how synaptic transmission is altered during sleep states relative to awake states (Segal, 1978; Winson & Abzug, 1977, 1978a, 1978b). By stimulating the perforant pathway, Winson and Abzug (1977) examined

how behavioral states affect synaptic transmission in the ipsilateral monosynaptic (entorhinal cortex (EC) to dentate gyrus (DG)), disynaptic (EC to DG to CA3) and trisynaptic pathway (EC to DG to CA3 to CA1). They found that in all three regions (i.e., DG, CA3, and CA1) the population spiking activity was higher during NREM state than during any other brain state. In addition, the fEPSP size of the trisynaptic response in the CA1 region was also higher during NREM. Similarly, the CA1 fEPSP response to activation of the contralateral CA1, was also higher during NREM sleep (Segal, 1978). Our results in mice show that, similar to the rat studies, the commissural CA1 pathway synaptic transmission is enhanced during NREM sleep. In addition, we found that the NREM/awake ratio of fEPSP slopes tightly cluster around a mean value of 1.3 (Fig. 4F). Thus, irrespective of the size of the awake-period fEPSP responses, in the NREM state, they get scaled by a roughly constant factor. Hence, the aggregate of mechanisms underlying the NREM effect can be conceptualized as a multiplicative gain modulation.

Considered as an evolutionary precursor to the corpus callosum, the hippocampal commissures have been retained in all mammals (Suárez et al., 2014), indicating their computational necessity. Although the functions of hippocampal commissures are largely unknown, one of the proposed functions of the corpus callosum is to integrate lateralized functions across the hemispheres (Aboitiz & Montiel, 2003; Bloom & Hynd, 2005). Given that functional specialization of the left and right hippocampus has been reported in rodents (Jordan, 2020), it is possible that the hippocampal commissures may integrate the lateralized functions recruited during the fear-conditioning task. The plasticity we observed may thus indicate a stronger integration of those functions contributing to the important memory process.

Methods

Animals

Wild type male C57BL/6J mice (Jackson Laboratory, stock number: 000664) were group-housed until they were at least 2 months old with unrestricted food and water. They were single-housed after implantation of the microdrive for neural recordings. All experiments were done during the animals' dark phase (12 h reverse light/dark cycle, lights off at 9 AM). All procedures and animal care were carried out in compliance with guidelines specified by the Institutional Animal Care and Use Committee at the University of Pennsylvania.

Microdrive assembly

A depth-adjustable microdrive carrying a stimulating electrode and multiple recording electrodes was custom-designed in SolidWorks CAD software to be lightweight and 3D-printed. The stimulating electrode consisted of an insulated tungsten wire that passed through and extended 1.1 mm out of a 28G stainless steel tube (tungsten wire: PFA coated, 51 μm core dia, 102 μm outer dia, A-M Systems). This length was chosen so that when the tip of the tungsten wire reaches the pyramidal cell layer of the dorsal hippocampus, the 28G tube would be in contact with the top part of the cortex directly above the hippocampus. The 28G tube acted as the current return path. Note that in this arrangement, the positive (28G tube) and negative (tungsten wire tip) terminals are spaced apart in the dorsal-ventral direction while remaining concentric with respect to their centers. This arrangement gave a much narrower stimulation artifact compared to twisted bipolar electrodes that had the positive and negative terminals close to each other. To minimize tissue damage, tetrodes were used as recording electrodes. They were made by twisting four insulated Nichrome wires (California Fine wires, Stablohm 800A, material #100189, 12.7 μm core, 20 μm outer dia, heavy polyimide coated). The four terminals were shorted together, and gold plated (to 100 – 300 KΩ impedance), thereby becoming a single recording channel. For easily penetrating the brain, the tips of the stimulating and recording electrodes were cut at a 45 deg angle. Along with the electrodes, ground and reference wires (insulated silver wires, PFA coated, 127 μm core dia, 178 μm outer dia, stripped at the terminals, A-M Systems), were connected to a light-weight electrode interphase board (modified EIB-18, Neuralynx Inc). The electrodes were carried on a shuttle, movable by screws. The microdrive weighed < 1g when assembled (~1.5g on the mouse head with added dental cement). In several mice, a non-adjustable version of this microdrive was used.

Surgical procedures

Anesthesia was induced by 3% isoflurane. Once the animals stopped moving, isoflurane was reduced and maintained at ~2% for another 5 min. Then animals were transferred from the anesthesia induction box to the stereotaxic frame where isoflurane was maintained at 1.75 - 2.25% with progressive reduction of the isoflurane level every hour. The flow rate was 1 L/min. Burr holes were drilled into the skull at AP: -1.7, ML: -1.25 relative to Bregma (Franklin & Paxinos, 2008) for stimulating and at AP: -1.7, ML: +1.25 for the center of the array of the recording electrodes. A ground screw (Antrin Miniature specialists) was threaded on the bone plate over the right cerebellum (interparietal bone) and secured by Loctite superglue. The ground silver wire (insulation stripped for 1.5cm near the tip) was tightly wound around the ground screw and further secured by covering it with silver paint (Silver Print, CRC). A burr hole was made over the left frontal bone and the reference wire (silver ball tip) was inserted under the bone, over the brain surface. When implanting depth-adjustable microdrives, the stimulating and recording electrodes were lowered to DV: -1.0 during surgery; further adjustments to the final target were made 2-3 days after surgery. For non-adjustable microdrives, the stimulating and recording electrodes were placed at their final locations identified by neural recording during surgery and adjusting the electrodes until the maximal stimulation response on most recording electrodes was obtained. The

microdrive was secured to the skull using C & B MetaBond (Parkell) dental cement that bonded the implant to the skull strongly, obviating the need for any additional skull screws.

Recording procedure

Pre-experimental procedures: Mice with non-adjustable microdrives were left undisturbed for at least one week for recovery from the surgery and to allow the electrodes to reach a stable location. After this, mice were habituated to the recording procedure for at least 3 days before experiments began. For mice with adjustable microdrives, after the surgery, we waited for a minimum of 2 days after which the mice were brought to the recording room and the electrodes were lowered by a maximum of 80 μm per day. The characteristic reversal of fEPSP polarity in the pyramidal cell layer along with increased spiking activity was used as a guide to reach the *stratum radiatum*. After that, we waited at least a day to let the electrodes settle. Placing the mouse on top of a tall (6 in) coffee cup (top covered with paper towel), allowed us to quickly connect the head-stage preamplifiers without stress to the mouse. Securing the mouse by holding the microdrive itself, also helped avoid touching the mouse directly. Recordings were done in the dark in the home cage placed inside a sound-attenuating enclosure (Med Associates). The bedding and nest in the home cage were left undisturbed. To avoid tangling of recording cable, the water bottle was removed but a few food pellets were moistened to minimize dehydration of the mouse. To stop the mice from climbing out of the home cage, we stacked another cage with its bottom removed, on top of the home cage. For free movement and to reduce the weight added to the head, we used lightweight and flexible recording wires (HS-18 head stage with Cooner wire, Neuralynx) and a motorized commutator (Saturn, Neuralynx) that untwisted the wire. The AC-coupled broad band (0.1 Hz to 16KHz) signal was continuously recorded at a sampling rate of 32 KHz using the Neuralynx Digital Lynx SX system. Stimulus pulses (100μs) were generated by an A-M systems 2100 stimulus isolator with Master-9 pulser (AMPI) periodically giving pulse triggers. Video was acquired at 30 frames/s, and synchronized with the neural recording.

Neural recording and behavior: At the time of the experiments, mice were ~ 3 months old (median = 3.3 months, lower-upper quartiles: 2.95 – 3.8 months). The baseline fEPSP measurement began ~1.5h (median; lower-upper quartile: 1.3 – 1.9h) after the house light was turned off. For monitoring synaptic strength, we chose a stimulation current intensity that elicited 40-50% of the maximal response based on an input-output curve, where a set of 5-7 current intensities ranging from 15 to 70 μA were given in a random order, with each current level repeated 3 times. A sigmoidal function was fit to this data from which we computed the 40-50% of maximal response. This current level was used throughout the day. Following this procedure, baseline measurement began using a stimulus pulse (100 μs, monophasic, square shape) that was given every 60s, for 2 hours. After this, the recording was stopped, and the mouse was disconnected. The mouse was then carried in its home cage to the fear conditioning chamber (Coulbourn Instruments), which had been cleaned with 20% ethanol. The conditioning consisted of a 2-minute exploration of the shock chamber after which the mouse received 5 foot-shocks with a 30 s interval between them. Each shock was given at 0.6 mA for 1 s (8-pole scrambled square-wave foot-shock, 40 Hz repetition rate, Coulbourn Precision animal shocker H13-15). After the last shock the mouse remained in the chamber for 30 s. To avoid handling-stress to the mouse, after the shocking procedure, instead of capturing the mouse by hand, we used a cardboard scoop ("shepherd shacks" used for mice) on to which the mice easily entered. We returned the mouse to his home cage for recording and continued the stimulation pulses as in the baseline for another 3 hours. Memory retention was tested either 24h later (n = 12) or after 7 (n = 9) or more days (n = 3, one mouse each after 8, 10 and 27 days) by measuring freezing (FreezeFrame, Actimetrics) in the original shocked chamber for 5 min. The mouse group that was tested 7 or more days after training is referred to as the 7-day post-conditioning group in the Results section.

Histology

To localize the electrode tips, we first anesthetized the mouse with ketamine-xylazine mixture and passed 30 μA positive current for 8-10 s through the electrode tips with the ground or reference as the current return path. Cardiac perfusion was then performed with 10% formalin (in phosphate-buffered saline) fixative. The mouse head with the microdrive implant was submerged inside the fixative at 4℃ for at least 1 day. After that, leaving the region of skull cemented to the implant intact, the rest of the tissue surrounding the brain was carefully removed. Finally, the brain was gently separated out of the skull/implant and fixed in 10% formalin for another day. The brain was then sliced coronally at 50 μm thickness in a vibratome.

Data analysis

All data analyses were carried out using custom-written MATLAB code and the large-scale data management framework – DataJoint (Yatsenko et al., 2015).

Slope measurement of the fEPSP: First, the broadband signal was down-sampled to 16 KHz and filtered at 0.1 – 5000 Hz using MATLAB's decimate routine. The fEPSP stimulation response traces were then extracted using the stimulation onset timestamps. To compute the slope of the initial downward deflection, a second derivative of the trace was computed. This derivative had a single prominent peak at the time when the downward deflection was roughly halfway down. We then placed a 500 ms window centered on the time of the derivative's peak and computed the slope from the raw trace in this time window.

Motion estimation: The mouse's position was detected online by thresholding the red LED tracker lights attached to the head-stage preamplifiers. A motion index (m) was computed using the following heuristic formula based on the robust estimate of standard deviation (Quiroga, Nadasdy, & Ben-Shaul, 2004) of the x and y coordinates ($\boldsymbol{x}, \boldsymbol{y}$) of 5 s contiguous time windows (5s x 30fps = 150 pairs of data points):

$$m = s(\boldsymbol{x})^2 + s(\boldsymbol{y})^2, where \qquad 1$$
$$s(\boldsymbol{x}) = median(|\boldsymbol{x} - median(\boldsymbol{x})|)/0.6745$$
$$s(\boldsymbol{y}) = median(|\boldsymbol{y} - median(\boldsymbol{y})|)/0.6745$$

The median-based robust standard deviation was employed for the following reasons. The position tracker software sometimes mistakenly detected the reflection of the tracker LED on the sidewalls of the mouse cage as the position of the mouse. At other times, the recording cable or the nest of the mouse blocked the LED from the view of the camera resulting in loss of mouse position; the tracking software assigns a position of (0,0) in these cases. All these artifacts result in sudden jumps in the otherwise smoothly changing values of the x and y coordinates. By employing median, we minimized the contribution of these artifacts thereby avoiding overestimation of the motion index.

Identification of behavioral states*:* Behavioral states were identified manually by combining mouse motion information with the hippocampal theta/delta band power ratio, as done previously (Grosmark et al., 2012). Power in the theta band (4-11Hz) and delta band (1-4 Hz) was computed in 5 s contiguous time windows using *bandpower* routine of MATLAB (MathWorks, MA). NREM states were identified by the lack of animal motion along with a sustained decrease in theta/delta power ratio. The REM state was identified by lack of animal motion along with a sustained increase in the theta/delta ratio. The time segments outside of NREM and REM states were treated as the awake state. For the spectrogram in Figure 3B, we computed continuous wavelet transform in MATLAB using complex Morlet wavelets (Supplemental materials).

Inclusion criteria for mice and electrodes: Electrodes that were outside the CA1 region were excluded. In addition, to get reliable slope estimates, electrodes in the CA1 that had weak stimulation

responses (fEPSP peak magnitude less than ~0.5 mV) were also excluded. Similarly, electrodes that landed near the pyramidal cell layer were also excluded because they often showed a popspike, which makes the slope measurement unreliable. In addition, electrodes with slope values that showed systematic drift (i.e., were not stable) during the baseline (see the Baseline stability testing section below) were excluded (0/62 in the cFC group and 2/25 in the sham-conditioning group). Mice without any stable electrodes were also excluded (0/24 in the cFC group and 1/13 in the sham-conditioning group).

Baseline stability testing: A stable baseline of synaptic strength is a prerequisite for a valid interpretation of the post-conditioning synaptic changes. Therefore, we defined the baseline stability at the individual electrode and at the population level. First, at the individual electrode level, if the baseline drifts up in some electrodes and drifts down in others, they can cancel out each other at the population level, resulting in a 'steady' average baseline. Hence, we tested stability of individual electrodes as described in the next section. It is also possible that in most or all electrodes there may be a small drift in the same direction. In that case, the electrode-level test will fail to identify drift adequately; whereas at the population level, these small effects will add up to be easily detectable. Therefore, we also performed stability tests on the average across electrodes (see *Statistical tests for learning effect* section).

Single electrode level stability test: To test for baseline stability in a principled way, we used the following statistical procedure on the Kolmogorov-Smirnov (KS) statistic that quantifies the distance between the empirical distribution function of a sample and the cumulative distribution function of a reference (null) distribution. The normalized fEPSP slope data (sleep segments removed) ordered in time is the sample distribution, the cumulative sum of which forms the empirical distribution function (F). Then, we created a reference distribution that denotes a perfectly stable baseline with no change in fEPSP slope over time. As an ideal stable baseline would have 100% as the value of normalized fEPSP slope at each time point, we created such a sequence where each element was 100. The length of this sequence was the same as that of the experimentally measured fEPSP slope data. The cumulative sum of the ideal stable baseline data points formed the reference distribution function (F_n). As a test statistic (D), similar to the KS statistic, we computed the maximal absolute distance between the two distribution functions (F and F_n). To find if this statistic is significant, we created a null distribution by bootstrapping, where we repeated the computation of the test statistic (D^*) 10,000 times, each time randomly picking the same number of fEPSP slope data points as the original data (resampling with replacement). Such shuffling results in a sequence of fEPSP slope data that does not have systematic drift over time but preserves the noise in the data. We then computed the fraction of bootstrapped D^* values that were above D, as the p-value. We treated any p-value less than 0.05 as indicative of a significant drift of the slope data. Electrodes with such fEPSP slopes were considered unstable.

Statistical tests for learning effect: We sought out a statistical procedure that can test stability of the baseline and the learning-related changes more comprehensively with the ability to handle missing data. We opted for the linear mixed model (LMM) formulated for analyzing interrupted time series. We treated fEPSP slope data points as an interrupted time series (Wagner et al., 2002) where the baseline time series is "interrupted" by fear conditioning. A linear fit was applied to the baseline and post-conditioning fEPSP slopes (segmented linear regression, see Supplemental materials). The linear fit contained two types of parameters – intercept and gain. Note that, the term 'gain' is used instead of 'slope' to refer to the slope of the line fit; this avoids the slope of the fEPSP being confused with the slope of the line fit.

The intercept denotes the level on the y-axis at which the fEPSP slopes start at the beginning of the baseline or at the beginning of the post-conditioning period. Learning may result in an abrupt "jump" or increase in the fEPSP slopes at the beginning of the post-conditioning period (Fig. 2E & Fig. 4G). A significant increase in the intercept parameter in the post-conditioning period relative to baseline thus reflects a significant increase in post-conditioning fEPSP slopes.

The gain value indicates whether the fEPSP slopes remain stable (zero gain), grow (positive gain) or decline (negative gain) over time. For example, for the baseline period, a gain value that is not significantly different from zero indicates that the baseline is stable (Fig. 2E, Fig. 4G and Fig. 5D). A positive gain value of the fit to the post-conditioning period will indicate that the fEPSP slopes grow further with time relative to those of the baseline (Fig. 2E).

LMM analyses were done in the SPSS statistical software package PASW-18. Briefly, the subjects (mice) were treated as random effects and time points of baseline and post-conditioning periods were treated as fixed effects. The normalized fEPSP slope was used as the dependent variable. Although for the display purposes the raw data points were 5-min binned in Fig. 2E, Fig. 4G-H and Fig. 5D, for statistical tests, the non-binned raw normalized fEPSP slopes were used. For example, for statistical tests of Fig. 2E, the baseline had 120 data points per mouse. Note that we treated the first 10 min of the post-conditioning period as a transition period. To avoid modeling this transition that would require additional model parameters, we excluded the data (10 data points) corresponding to this period during statistical tests.

Data availability

Raw data and MATLAB code associated with this study are available at (datadryad doi link here)

Acknowledgements

We thank Shannon Wolfman and Daniel Kalamarides for their thorough feedback on the manuscript, Dimitri Yatsenko for help with statistical methods, Marion Scott for technical and administrative assistance, Tiffany Brown-Mangum and Tyisha Hundley for their help with animal husbandry. This work was supported by National Institutes of Health grants R01AA026267 (National Institute on Alcohol Abuse and Alcoholism, J.A.D.) and R01NS021229 (National Institute of Neurological Disorders and Stroke, J.A.D.). This work also was supported by a generous award from the Chernowitz Medical Research Foundation.

References

Abel, T., Havekes, R., Saletin, J. M., & Walker, M. P. (2013). Sleep, plasticity and memory from molecules to whole-brain networks. *Curr Biol, 23*(17), R774-788. doi:10.1016/j.cub.2013.07.025

Aboitiz, F., & Montiel, J. (2003). One hundred million years of interhemispheric communication: the history of the corpus callosum. *Braz J Med Biol Res, 36*(4), 409-420. doi:10.1590/s0100-879x2003000400002

Ambrosini, M. V., Mariucci, G., Colarieti, L., Bruschelli, G., Carobi, C., & Giuditta, A. (1993). The Structure of Sleep is Related to the Learning Ability of Rats. *European Journal of Neuroscience, 5*(3), 269-275. doi:10.1111/j.1460-9568.1993.tb00493.x

Bear, M. F. (1996). A synaptic basis for memory storage in the cerebral cortex. *Proceedings of the National Academy of Sciences, 93*(24), 13453-13459. doi:10.1073/pnas.93.24.13453

Bliss, T. V., Lancaster, B., & Wheal, H. V. (1983). Long-term potentiation in commissural and Schaffer projections to hippocampal CA1 cells: an in vivo study in the rat. *The Journal of physiology, 341*, 617-626. doi:10.1113/jphysiol.1983.sp014828

Bloom, J. S., & Hynd, G. W. (2005). The Role of the Corpus Callosum in Interhemispheric Transfer of Information: Excitation or Inhibition? *Neuropsychology Review, 15*(2), 59-71. doi:10.1007/s11065-005-6252-y

Bonnet, C., Léger, L., Baubet, V., Debilly, G., & Cespuglio, R. (1997). Influence of a 1 h immobilization stress on sleep states and corticotropin-like intermediate lobe peptide (CLIP or ACTH18–39, Ph-ACTH18–39) brain contents in the rat. *Brain Research, 751*(1), 54-63. doi:https://doi.org/10.1016/S0006-8993(96)01390-X

Bramham, C. R., Maho, C., & Laroche, S. (1994). Suppression of long-term potentiation induction during alert wakefulness but not during 'enhanced' REM sleep after avoidance learning. *Neuroscience, 59*(3), 501-509. doi:https://doi.org/10.1016/0306-4522(94)90172-4

Broussard, J. I., Yang, K., Levine, A. T., Tsetsenis, T., Jenson, D., Cao, F., . . . Dani, J. A. (2016). Dopamine Regulates Aversive Contextual Learning and Associated In Vivo Synaptic Plasticity in the Hippocampus. *Cell Rep, 14*, 1-10. doi:http://dx.doi.org/10.1016/j.celrep.2016.01.070

Buffington, S. A., Huang, W., & Costa-Mattioli, M. (2014). Translational Control in Synaptic Plasticity and Cognitive Dysfunction. *Annu Rev Neurosci, 37*(1), 17-38. doi:10.1146/annurev-neuro-071013-014100

Buzsáki, G. (2015). Hippocampal sharp wave-ripple: A cognitive biomarker for episodic memory and planning. *Hippocampus, 25*(10), 1073-1188. doi:10.1002/hipo.22488

Buzsaki, G., Grastyan, E., Czopf, J., Kellenyi, L., & Prohaska, O. (1981). Changes in neuronal transmission in the rat hippocampus during behavior. *Brain Res, 225*(2), 235-247. doi:https://doi.org/10.1016/0006-8993(81)90833-7

Buzsáki, G., Lai-Wo S, L., & Vanderwolf, C. H. (1983). Cellular bases of hippocampal EEG in the behaving rat. *Brain Research Reviews, 6*(2), 139-171. doi:https://doi.org/10.1016/0165-0173(83)90037-1

Chrobak, J. J., & Buzsáki, G. (1996). High-frequency oscillations in the output networks of the hippocampal-entorhinal axis of the freely behaving rat. *J Neurosci, 16*(9), 3056-3066. doi:10.1523/jneurosci.16-09-03056.1996

Cullen, P. K., Gilman, T. L., Winiecki, P., Riccio, D. C., & Jasnow, A. M. (2015). Activity of the anterior cingulate cortex and ventral hippocampus underlie increases in contextual fear generalization. *Neurobiology of Learning and Memory, 124*, 19-27. doi:https://doi.org/10.1016/j.nlm.2015.07.001

Datta, S. (2000). Avoidance task training potentiates phasic pontine-wave density in the rat: A mechanism for sleep-dependent plasticity. *The Journal of neuroscience : the official journal of the Society for Neuroscience, 20*(22), 8607-8613. doi:10.1523/JNEUROSCI.20-22-08607.2000

del C. Gonzalez, M. M., Debilly, G., Valatx, J.-L., & Jouvet, M. (1995). Sleep increase after immobilization stress: role of the noradrenergic locus coeruleus system in the rat. *Neuroscience Letters, 202*(1), 5-8. doi:https://doi.org/10.1016/0304-3940(95)12209-5

Donlea, J. M., Thimgan, M. S., Suzuki, Y., Gottschalk, L., & Shaw, P. J. (2011). Inducing Sleep by Remote Control Facilitates Memory Consolidation in Drosophila. *Science, 332*(6037), 1571-1576. doi:10.1126/science.1202249

dos Santos Corrêa, M., Vaz, B. d. S., Grisanti, G. D. V., de Paiva, J. P. Q., Tiba, P. A., & Fornari, R. V. (2019). Relationship between footshock intensity, post-training corticosterone release and contextual fear memory specificity over time. *Psychoneuroendocrinology, 110*, 104447. doi:https://doi.org/10.1016/j.psyneuen.2019.104447

Eichenbaum, H. (2016). Still searching for the engram. *Learning & behavior, 44*(3), 209-222. doi:10.3758/s13420-016-0218-1

Franklin, K. B. J., & Paxinos, G. (2008). *The mouse brain in stereotaxic coordinates*. Amsterdam: Elsevier.

Girardeau, G., Benchenane, K., Wiener, S. I., Buzsáki, G., & Zugaro, M. B. (2009). Selective suppression of hippocampal ripples impairs spatial memory. *Nature Neuroscience, 12*(10), 1222-1223. doi:10.1038/nn.2384

Girardeau, G., Inema, I., & Buzsáki, G. (2017). Reactivations of emotional memory in the hippocampus–amygdala system during sleep. *Nature Neuroscience, 20*(11), 1634-1642. doi:10.1038/nn.4637

Graves, L. A., Heller, E. A., Pack, A. I., & Abel, T. (2003). Sleep deprivation selectively impairs memory consolidation for contextual fear conditioning. *Learn Mem, 10*(3), 168-176. doi:10.1101/lm.48803

Green, E. J., McNaughton, B. L., & Barnes, C. A. (1990). Exploration-dependent modulation of evoked responses in fascia dentata: dissociation of motor, EEG, and sensory factors and evidence for a synaptic efficacy change. *J Neurosci, 10*(5), 1455-1471. doi:10.1523/jneurosci.10-05-01455.1990

Grosmark, A. D., Mizuseki, K., Pastalkova, E., Diba, K., & Buzsáki, G. (2012). REM sleep reorganizes hippocampal excitability. *Neuron, 75*(6), 1001-1007. doi:10.1016/j.neuron.2012.08.015

Gruart, A., Munoz, M. D., & Delgado-Garcia, J. M. (2006). Involvement of the CA3-CA1 synapse in the acquisition of associative learning in behaving mice. *J Neurosci, 26*(4), 1077-1087. doi:10.1523/JNEUROSCI.2834-05.2006

Hellman, K., & Abel, T. (2007). Fear conditioning increases NREM sleep. *Behav Neurosci, 121*(2), 310-323. doi:10.1037/0735-7044.121.2.310

Hulse, B. K., Lubenov, E. V., & Siapas, A. G. (2017). Brain State Dependence of Hippocampal Subthreshold Activity in Awake Mice. *Cell Rep, 18*(1), 136-147. doi:10.1016/j.celrep.2016.11.084

Jarosiewicz, B., McNaughton, B. L., & Skaggs, W. E. (2002). Hippocampal population activity during the small-amplitude irregular activity state in the rat. *J Neurosci, 22*(4), 1373-1384.

Johansen, Joshua P., Cain, Christopher K., Ostroff, Linnaea E., & LeDoux, Joseph E. (2011). Molecular Mechanisms of Fear Learning and Memory. *Cell, 147*(3), 509-524. doi:10.1016/j.cell.2011.10.009

Joo, H. R., & Frank, L. M. (2018). The hippocampal sharp wave-ripple in memory retrieval for immediate use and consolidation. *Nat Rev Neurosci, 19*(12), 744-757. doi:10.1038/s41583-018-0077-1

Jordan, J. T. (2020). The rodent hippocampus as a bilateral structure: A review of hemispheric lateralization. *Hippocampus, 30*(3), 278-292. doi:10.1002/hipo.23188

Karunakaran, S., Chowdhury, A., Donato, F., Quairiaux, C., Michel, C. M., & Caroni, P. (2016). PV plasticity sustained through D1/5 dopamine signaling required for long-term memory consolidation. *Nat Neurosci*. doi:10.1038/nn.4231

Kay, K., Sosa, M., Chung, J. E., Karlsson, M. P., Larkin, M. C., & Frank, L. M. (2016). A hippocampal network for spatial coding during immobility and sleep. *Nature, 531*(7593), 185-190. doi:10.1038/nature17144

Kemp, A., & Manahan-Vaughan, D. (2004). Hippocampal long-term depression and long-term potentiation encode different aspects of novelty acquisition. *Proceedings of the National Academy of Sciences of the United States of America, 101*(21), 8192-8197. doi:10.1073/pnas.0402650101

Klinzing, J. G., Niethard, N., & Born, J. (2019). Mechanisms of systems memory consolidation during sleep. *Nat Neurosci, 22*(10), 1598-1610. doi:10.1038/s41593-019-0467-3

Koehl, M., Bouyer, J. J., Darnaudéry, M., Le Moal, M., & Mayo, W. (2002). The effect of restraint stress on paradoxical sleep is influenced by the circadian cycle. *Brain Res, 937*(1-2), 45-50. doi:10.1016/s0006-8993(02)02463-0

Laurberg, S. (1979). Commissural and intrinsic connections of the rat hippocampus. *J Comp Neurol, 184*(4), 685-708. doi:10.1002/cne.901840405

Lesting, J., Daldrup, T., Narayanan, V., Himpe, C., Seidenbecher, T., & Pape, H.-C. (2013). Directional Theta Coherence in Prefrontal Cortical to Amygdalo-Hippocampal Pathways Signals Fear Extinction. *PLoS One, 8*(10), e77707. doi:10.1371/journal.pone.0077707

Likhtik, E., Stujenske, J. M., A Topiwala, M., Harris, A. Z., & Gordon, J. A. (2013). Prefrontal entrainment of amygdala activity signals safety in learned fear and innate anxiety. *Nat Neurosci, 17*, 106-106. doi:10.1038/nn.3582

Malenka, R. C., & Bear, M. F. (2004). LTP and LTD: an embarrassment of riches. *Neuron, 44*(1), 5-21. doi:10.1016/j.neuron.2004.09.012

Maren, S., Phan, K. L., & Liberzon, I. (2013). The contextual brain: implications for fear conditioning, extinction and psychopathology. *Nat Rev Neurosci, 14*(6), 417-428. doi:10.1038/nrn3492

Martin, S. J., Shires, K. L., & da Silva, B. M. (2019). Hippocampal Lateralization and Synaptic Plasticity in the Intact Rat: No Left-Right Asymmetry in Electrically Induced CA3-CA1 Long-Term Potentiation. *Neuroscience, 397*, 147-158. doi:10.1016/j.neuroscience.2018.11.044

Mavanji, V., Siwek, D. F., Patterson, E. H., Spoley, E. E., & Datta, S. (2003). Effects of passive-avoidance training on sleep-wake state-specific activity in the basolateral and central nuclei of the amygdala. *Behav Neurosci, 117*(4), 751-759. doi:10.1037/0735-7044.117.4.751

Mizuseki, K., Diba, K., Pastalkova, E., & Buzsáki, G. (2011). Hippocampal CA1 pyramidal cells form functionally distinct sublayers. *Nature Neuroscience, 14*(9), 1174-1181. doi:10.1038/nn.2894

Moita, M. A., Rosis, S., Zhou, Y., LeDoux, J. E., & Blair, H. T. (2004). Putting fear in its place: remapping of hippocampal place cells during fear conditioning. *J Neurosci, 24*(31), 7015-7023. doi:10.1523/JNEUROSCI.5492-03.2004

Narayanan, R. T., Seidenbecher, T., Sangha, S., Stork, O., & Pape, H. C. (2007). Theta resynchronization during reconsolidation of remote contextual fear memory. *Neuroreport, 18*(11), 1107-1111. doi:10.1097/WNR.0b013e3282004992

Nicoll, R. A. (2017). A Brief History of Long-Term Potentiation. *Neuron, 93*(2), 281-290. doi:10.1016/j.neuron.2016.12.015

O'Keefe, J. (1976). Place units in the hippocampus of the freely moving rat. *Experimental Neurology, 51*(1), 78-109. doi:https://doi.org/10.1016/0014-4886(76)90055-8

Ognjanovski, N., Maruyama, D., Lashner, N., Zochowski, M., & Aton, S. J. (2014). CA1 hippocampal network activity changes during sleep-dependent memory consolidation. *Front Syst Neurosci, 8*(61). doi:10.3389/fnsys.2014.00061

Ognjanovski, N., Schaeffer, S., Wu, J., Mofakham, S., Maruyama, D., Zochowski, M., & Aton, S. J. (2017). Parvalbumin-expressing interneurons coordinate hippocampal network dynamics required for memory consolidation. *Nat Commun, 8*, 15039-15039. doi:10.1038/ncomms15039 https://www.nature.com/articles/ncomms15039#supplementary-information

Olafsdottir, H. F., Bush, D., & Barry, C. (2018). The Role of Hippocampal Replay in Memory and Planning. *Curr Biol, 28*(1), R37-r50. doi:10.1016/j.cub.2017.10.073

Pape, H. C., Narayanan, R. T., Smid, J., Stork, O., & Seidenbecher, T. (2005). Theta activity in neurons and networks of the amygdala related to long-term fear memory. *Hippocampus, 15*(7), 874-880. doi:10.1002/hipo.20120

Pawlyk, A. C., Morrison, A. R., Ross, R. J., & Brennan, F. X. (2008). Stress-induced changes in sleep in rodents: models and mechanisms. *Neuroscience and biobehavioral reviews, 32*(1), 99-117. doi:10.1016/j.neubiorev.2007.06.001

Pedraza, L. K., Sierra, R. O., Boos, F. Z., Haubrich, J., Quillfeldt, J. A., & Alvares Lde, O. (2016). The dynamic nature of systems consolidation: Stress during learning as a switch guiding the rate of the hippocampal dependency and memory quality. *Hippocampus, 26*(3), 362-371. doi:10.1002/hipo.22527

Penn, A. C., Zhang, C. L., Georges, F., Royer, L., Breillat, C., Hosy, E., . . . Choquet, D. (2017). Hippocampal LTP and contextual learning require surface diffusion of AMPA receptors. *Nature, 549*(7672), 384-388. doi:10.1038/nature23658

Phelps, E. A., Hirst, W., & Gazzaniga, M. S. (1991). Deficits in Recall Following Partial and Complete Commissurotomy. *Cerebral Cortex, 1*(6), 492-491. doi:10.1093/cercor/1.6.492

Popa, D., Duvarci, S., Popescu, A. T., Lena, C., & Pare, D. (2010). Coherent amygdalocortical theta promotes fear memory consolidation during paradoxical sleep. *Proc Natl Acad Sci U S A, 107*(14), 6516-6519. doi:10.1073/pnas.0913016107

Quiroga, R. Q., Nadasdy, Z., & Ben-Shaul, Y. (2004). Unsupervised spike detection and sorting with wavelets and superparamagnetic clustering. *Neural Comput, 16*(8), 1661-1687. doi:10.1162/089976604774201631

Rampin, C., Cespuglio, R., Chastrette, N., & Jouvet, M. (1991). Immobilisation stress induces a paradoxical sleep rebound in rat. *Neurosci Lett, 126*(2), 113-118. doi:10.1016/0304-3940(91)90532-x

Rothschild, G., Eban, E., & Frank, L. M. (2017). A cortical-hippocampal-cortical loop of information processing during memory consolidation. *Nature Neuroscience, 20*(2), 251-259. doi:10.1038/nn.4457

Sacchetti, B., Lorenzini, C. A., Baldi, E., Bucherelli, C., Roberto, M., Tassoni, G., & Brunelli, M. (2001). Long-lasting hippocampal potentiation and contextual memory consolidation. *Eur J Neurosci, 13*(12), 2291-2298. doi:10.1046/j.0953-816x.2001.01609.x

Sanford, L. D., Fang, J., & Tang, X. (2003). Sleep after differing amounts of conditioned fear training in BALB/cJ mice. *Behavioural Brain Research, 147*(1), 193-202. doi:https://doi.org/10.1016/S0166-4328(03)00180-3

Sanford, L. D., Tang, X., Ross, R. J., & Morrison, A. R. (2003). Influence of shock training and explicit fear-conditioned cues on sleep architecture in mice: strain comparison. *Behav Genet, 33*(1), 43-58. doi:10.1023/a:1021051516829

Schimanski, L. A., Wahlsten, D., & Nguyen, P. V. (2002). Selective Modification of Short-Term Hippocampal Synaptic Plasticity and Impaired Memory Extinction in Mice with a Congenitally Reduced Hippocampal Commissure. *The Journal of Neuroscience, 22*(18), 8277-8286. doi:10.1523/jneurosci.22-18-08277.2002

Segal, M. (1978). A correlation between hippocampal responses to interhemispheric stimulation, hippocampal slow rhythmic activity and behaviour. *Electroencephalogr Clin Neurophysiol, 45*(3), 409-411. doi:10.1016/0013-4694(78)90192-x

Seidenbecher, T., Laxmi, T. R., Stork, O., & Pape, H. C. (2003). Amygdalar and hippocampal theta rhythm synchronization during fear memory retrieval. *Science, 301*(5634), 846-850. doi:10.1126/science.1085818

Shin, L. M., & Liberzon, I. (2010). The neurocircuitry of fear, stress, and anxiety disorders. *Neuropsychopharmacology, 35*(1), 169-191. doi:10.1038/npp.2009.83

Sirota, A., Montgomery, S., Fujisawa, S., Isomura, Y., Zugaro, M., & Buzsáki, G. (2008). Entrainment of neocortical neurons and gamma oscillations by the hippocampal theta rhythm. *Neuron, 60*(4), 683-697. doi:10.1016/j.neuron.2008.09.014

Smith, C., Young, J., & Young, W. (1980). Prolonged Increases in Paradoxical Sleep During and After A voidance-Task Acquisition. *Sleep, 3*(1), 67-81. doi:10.1093/sleep/3.1.67

Sporns, O. (2011). *Networks of the brain*: MIT Press.

Stäubli, U., & Scafidi, J. (1999). Time-Dependent Reversal of Long-Term Potentiation in Area CA1 of the Freely Moving Rat Induced by Theta Pulse Stimulation. *The Journal of Neuroscience, 19*(19), 8712-8719. doi:10.1523/jneurosci.19-19-08712.1999

Suárez, R., Gobius, I., & Richards, L. J. (2014). Evolution and development of interhemispheric connections in the vertebrate forebrain. *Frontiers in human neuroscience, 8*, 497-497. doi:10.3389/fnhum.2014.00497

Swanson, L. W., Wyss, J. M., & Cowan, W. M. (1978). An autoradiographic study of the organization of intrahippocampal association pathways in the rat. *J Comp Neurol, 181*(4), 681-715. doi:10.1002/cne.901810402

Tonegawa, S., Liu, X., Ramirez, S., & Redondo, R. (2015). Memory Engram Cells Have Come of Age. *Neuron, 87*(5), 918-931. doi:10.1016/j.neuron.2015.08.002

Wagner, A. K., Soumerai, S. B., Zhang, F., & Ross-Degnan, D. (2002). Segmented regression analysis of interrupted time series studies in medication use research. *J Clin Pharm Ther, 27*(4), 299-309. doi:10.1046/j.1365-2710.2002.00430.x

Walker, M. P., & Stickgold, R. (2006). Sleep, memory, and plasticity. *Annu Rev Psychol, 57*, 139-166. doi:10.1146/annurev.psych.56.091103.070307

Wang, M. E., Wann, E. G., Yuan, R. K., Ramos Alvarez, M. M., Stead, S. M., & Muzzio, I. A. (2012). Long-term stabilization of place cell remapping produced by a fearful experience. *J Neurosci, 32*(45), 15802-15814. doi:10.1523/JNEUROSCI.0480-12.2012

Wellman, L. L., Yang, L., Tang, X., & Sanford, L. D. (2008). Contextual Fear Extinction Ameliorates Sleep Disturbances Found Following Fear Conditioning in Rats. *Sleep, 31*(7), 1035-1042. doi:10.5665/sleep/31.7.1035

Whitlock, J. R., Heynen, A. J., Shuler, M. G., & Bear, M. F. (2006). Learning induces long-term potentiation in the hippocampus. *Science, 313*(5790), 1093-1097. doi:10.1126/science.1128134

Wilson, M., & McNaughton, B. (1994). Reactivation of hippocampal ensemble memories during sleep. *Science, 265*(5172), 676-679. doi:10.1126/science.8036517

Wiltgen, B. J., & Silva, A. J. (2007). Memory for context becomes less specific with time. *Learn Mem, 14*(4), 313-317. doi:10.1101/lm.430907

Wiltgen, B. J., Zhou, M., Cai, Y., Balaji, J., Karlsson, M. G., Parivash, S. N., . . . Silva, A. J. (2010). The Hippocampus Plays a Selective Role in the Retrieval of Detailed Contextual Memories. *Current Biology, 20*(15), 1336-1344. doi:https://doi.org/10.1016/j.cub.2010.06.068

Winson, J., & Abzug, C. (1977). Gating of neuronal transmission in the hippocampus: efficacy of transmission varies with behavioral state. *Science, 196*(4295), 1223-1225. doi:10.1126/science.193192

Winson, J., & Abzug, C. (1978a). Dependence upon behavior of neuronal transmission from perforant pathway through entorhinal cortex. *Brain Res, 147*(2), 422-427. doi:10.1016/0006-8993(78)90856-9

Winson, J., & Abzug, C. (1978b). Neuronal transmission through hippocampal pathways dependent on behavior. *J Neurophysiol, 41*(3), 716-732. doi:10.1152/jn.1978.41.3.716

Yatsenko, D., Reimer, J., Ecker, A. S., Walker, E. Y., Sinz, F., Berens, P., . . . Tolias, A. S. (2015). DataJoint: managing big scientific data using MATLAB or Python. *bioRxiv*, 031658. doi:10.1101/031658

Zhou, H., Xiong, G.-J., Jing, L., Song, N.-N., Pu, D.-L., Tang, X., . . . Xu, L. (2017). The interhemispheric CA1 circuit governs rapid generalisation but not fear memory. *Nat Commun, 8*(1), 2190-2190. doi:10.1038/s41467-017-02315-4

Figures

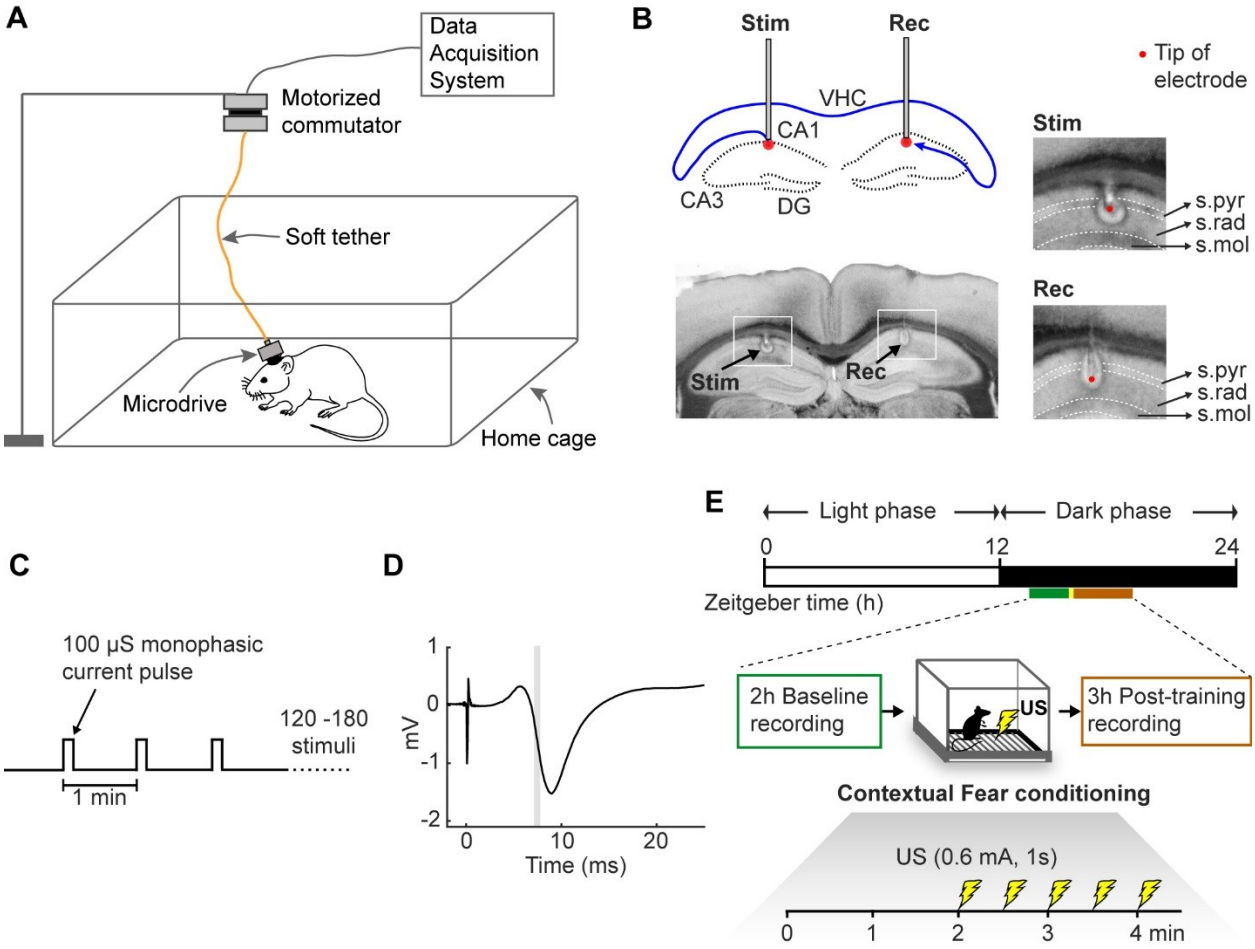

Figure 1. Experimental setup for measuring contextual fear conditioning (cFC)-related in vivo synaptic strength changes in the dorsal CA1 commissural pathway. ***A***, Illustration of field EPSP recordings conducted in the home cage of mice implanted with a lightweight microdrive carrying a stimulating electrode and multiple recording electrodes. The contents of the home cage such as food, bedding and nest are not depicted. ***B***, Top left: Schematic drawing showing the location of the stimulating (stim) and the recording (rec) electrodes, and the CA1-to-CA1 commissural pathway (blue) coursing through the ventral hippocampal commissure (VHC). Cell layers of CA1, CA3, and dentate gyrus (DG) are drawn as black dotted traces. Bottom left: Coronal brain section showing the stimulating and a recording electrode location in the CA1 identified by the electrolytic lesions seen as a "halo" around the electrode tips (marked by black arrows). The insets on the right are an expanded view of the stimulating and recording electrode locations with a red dot indicating the tip. Dotted white lines mark the boundaries of *stratum pyramidale* (s.pyr), *radiatum* (s.rad), and *moleculare* (s.mol). ***C***, Stimulation protocol applied to the left CA1, which was stimulated every 1 min with 100 µs square pulses for 2-3h. ***D***, Field EPSP response from the recording electrode shown in ***B***. Time zero marks the onset of the stimulus pulse. The slope measured in a 0.5 ms window (gray box) of the downward deflecting portion of the response was taken as a measure of synaptic strength. ***E***, The cFC procedure is didactically represented. Recording timelines are

represented on the Zeitgeber time scale (Zeitgeber time represents time (h) from the onset of house light). Experiments were conducted during the awake, dark phase. In the home cage, the synaptic strength was periodically measured as in ***C*** for 2 hours before (baseline), and 3 hours immediately after cFC. The green and orange bars under the Zeitgeber time scale represent baseline and post-conditioning recording periods respectively. The baseline measurement started ~1.5 h after the house light was turned off. The conditioning consisted of 2 min of exploration after which 5 foot-shocks (0.6mA, 1s), each separated by 30s, were delivered. US: unconditioned stimulus.

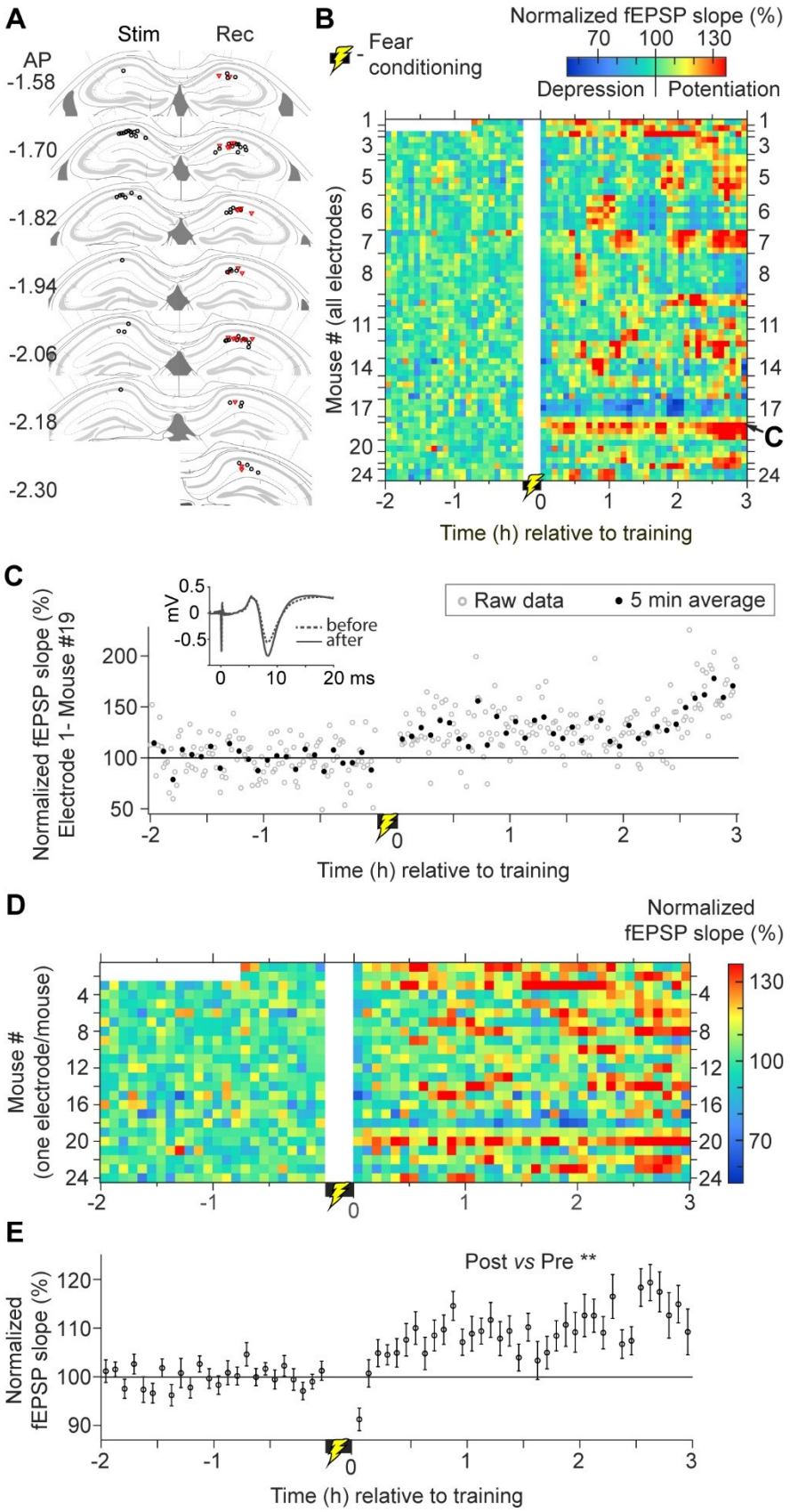
A
Stim
Rec
AP
-1.58
-1.70
-1.82
-1.94
-2.06
-2.18
-2.30
B
Fear conditioning
Normalized fEPSP slope (%)
70 100 130
Depression
Potentiation
Mouse # (all electrodes)
C
Time (h) relative to training
C
Normalized fEPSP slope (%)
Electrode 1- Mouse #19
Raw data
5 min average
mV
before
after
20 ms
Time (h) relative to training
D
Normalized fEPSP slope (%)
Mouse #
(one electrode/mouse)
E
Post vs Pre **
Normalized fEPSP slope (%)
Time (h) relative to training

Figure 2. In vivo synaptic strength modifications associated with cFC. ***A,*** The locations of the tips of the stimulating (stim) and recording (rec) electrodes were mapped onto a standard mouse atlas (Franklin and Paxinos, 2008). Red triangles indicate the single most potentiated electrode out of each mouse; those electrodes were used to indicate the largest measureable potentiation and were used in panels ***D*** & ***E***. ***B***, A heat map of the slopes of the fEPSP responses normalized to the baseline. Each row shows data from a single electrode. Rows between the adjacent ticks on the vertical axis indicate that a set of multiple electrodes was used to record from that particular mouse. The foot-shock conditioning period is marked by the yellow lightning bolt symbol near time zero. Mice #1 & 2 had only 45 min of baseline data. Mice # reflects the ascending chronological order of the recording dates. ***C***, The normalized slopes from the most potentiated electrode of the set used to record from mouse #19 in ***B***. The gray data points are the raw data, and the black points represent the 5-minute average of the raw data. The inset is the stimulation response averaged across all stimulation repetitions before (dotted trace) and after (continuous trace) fear conditioning. ***D,*** A heat map of the normalized fEPSP slopes from the most potentiated electrode set (red triangles in ***A***). ***E,*** The across-mouse average of the 5-min binned normalized slopes shown in ***D***. Error bars show SEM, and ** $p < 0.01$, is the significant increase in fEPSP slopes in the post-conditioning period relative to baseline.

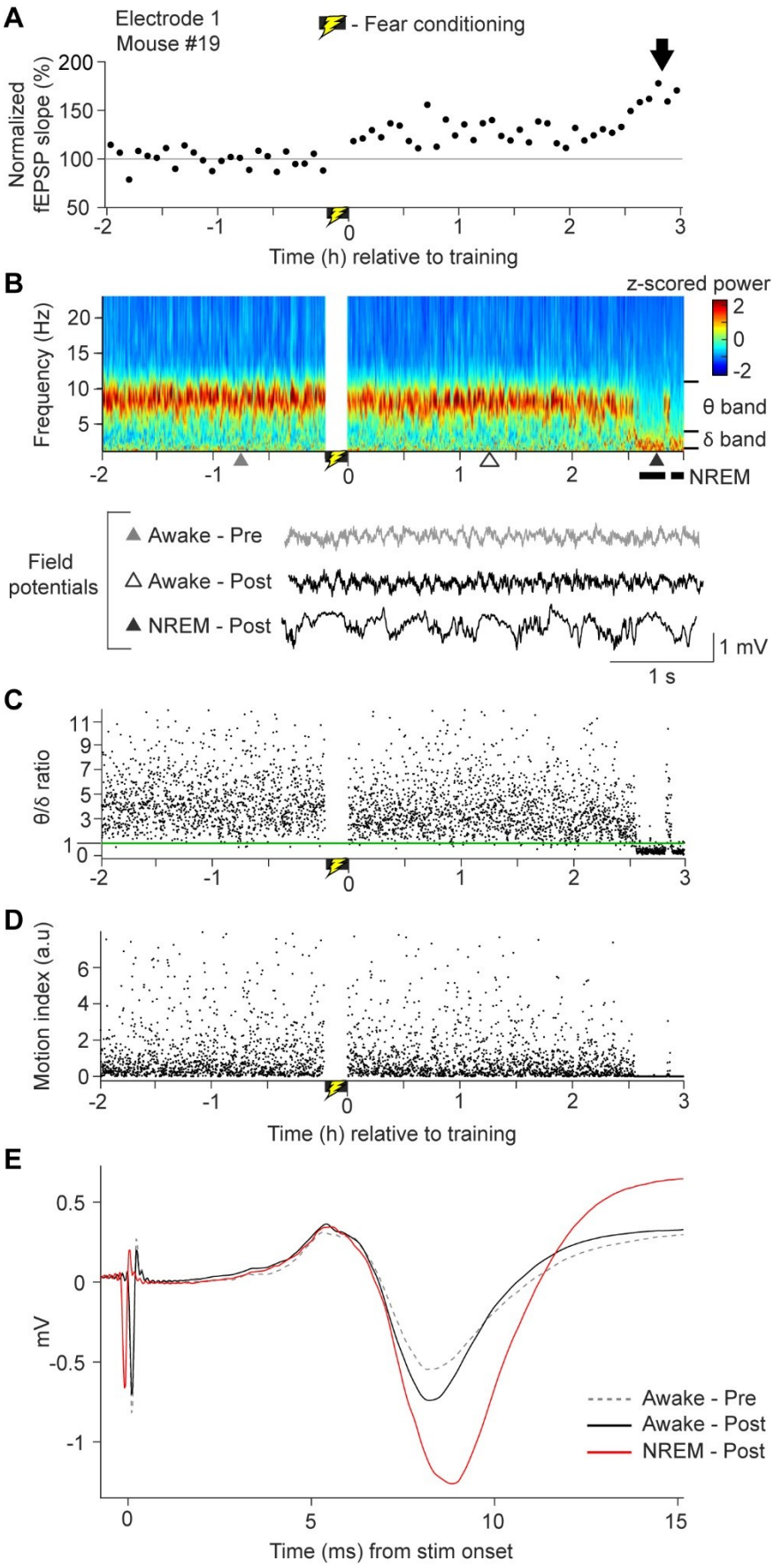
A
Electrode 1
Mouse #19
- Fear conditioning
Normalized fEPSP slope (%)
200
150
100
50
-2
-1
0
1
2
3
Time (h) relative to training
B
z-scored power
2
0
-2
Frequency (Hz)
20
15
10
5
θ band
δ band
NREM
Field potentials
Awake - Pre
Awake - Post
NREM - Post
1 mV
1 s
C
θ/δ ratio
11
9
7
5
3
1
0
D
Motion index (a.u)
6
4
2
0
Time (h) relative to training
E
mV
0.5
0
-0.5
-1
Awake - Pre
Awake - Post
NREM - Post
0
5
10
15
Time (ms) from stim onset

Figure 3. Fear conditioning associated NREM sleep and its effects on synaptic strength – single mouse example. The foot-shock conditioning period is marked by the yellow lightning bolt symbol near time zero. ***A,*** Normalized 5-min binned fEPSP slopes from a single electrode from mouse# 19 as in Figure **2*B***. The downward black arrow indicates an abrupt increase in synaptic potentiation in the last 30 min. ***B,*** Top: Spectrogram (z-scored across frequencies) of continuous broadband data from the electrode in ***A***. Black bars below the x-axis indicate the NREM periods. Theta frequency (θ, 5-11 Hz) and delta frequency (δ, 1-4 Hz) band boundaries are shown on the right. Bottom: Raw field potential traces of 4 s duration taken at time points marked by triangles at the bottom of the spectrogram. Scale bars at the bottom right apply to all three traces. ***C***, The ratio of power in the theta band over the delta band (θ/ δ) computed in 5-s contiguous time windows. ***D***, The motion index computed in 5-s contiguous time windows. a.u: arbitrary units. ***E*,** The average fEPSP responses during baseline (dotted trace), post-training awake period (black trace), and post-training NREM sleep period (red trace).

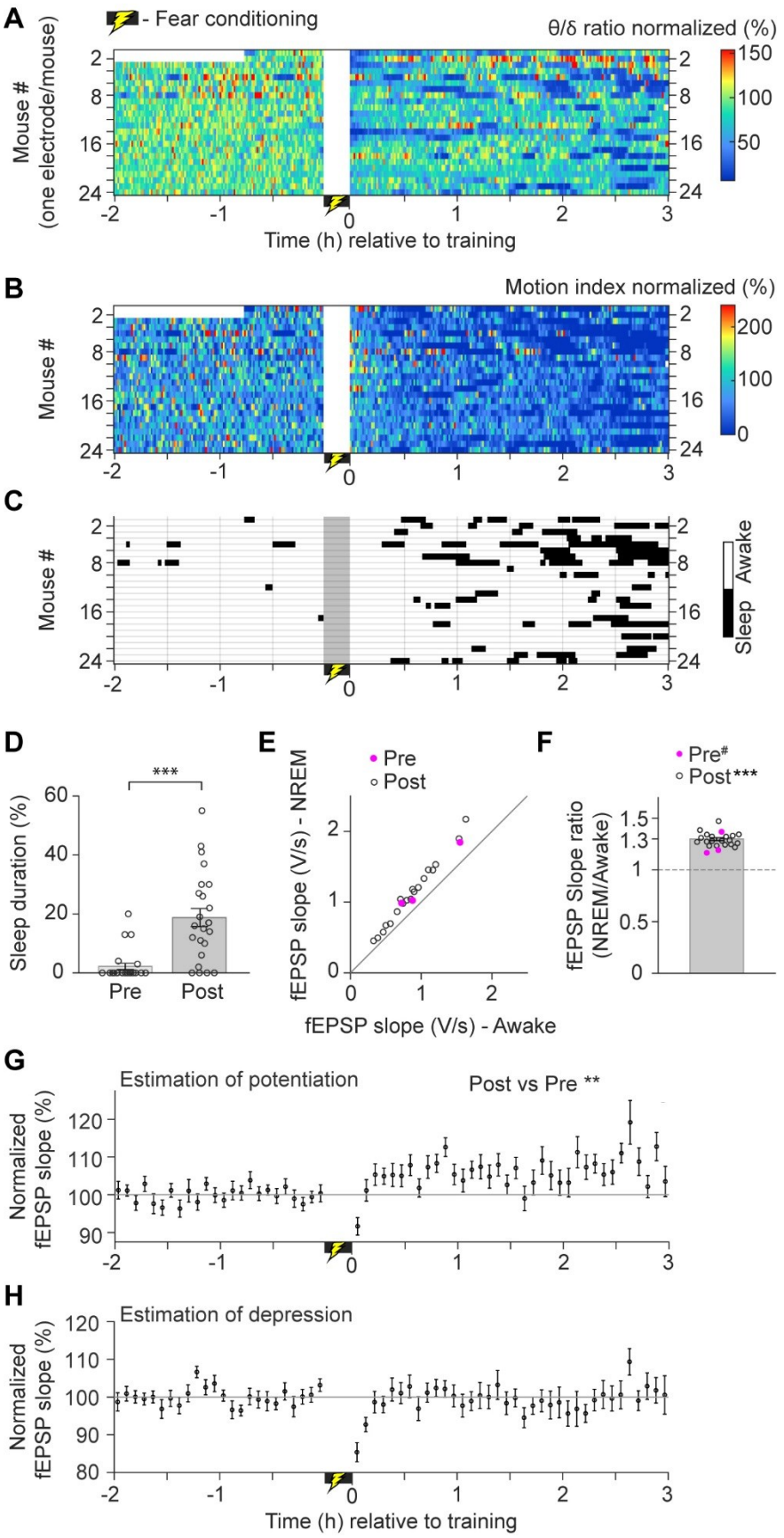
A
- Fear conditioning
θ/δ ratio normalized (%)
Mouse #
(one electrode/mouse)
Time (h) relative to training
B
Motion index normalized (%)
Mouse #
C
Mouse #
Awake
Sleep
D
Sleep duration (%)
***
Pre
Post
E
Pre
Post
fEPSP slope (V/s) - NREM
fEPSP slope (V/s) - Awake
F
Pre#
Post***
fEPSP Slope ratio
(NREM/Awake)
G
Estimation of potentiation
Post vs Pre **
Normalized
fEPSP slope (%)
H
Estimation of depression
Normalized
fEPSP slope (%)
Time (h) relative to training

Figure 4. Effect of NREM sleep on synaptic strength, and cFC-associated synaptic strength changes after accounting for sleep. The foot-shock conditioning period is marked by the yellow lightning bolt symbol near time zero. ***A-C***: Identification of sleep periods. ***A,*** Baseline-normalized theta/delta ratio computed in 5 s contiguous time windows. Each row corresponds to data from a maximally potentiated single electrode from each mouse (the same electrodes as in Fig. **2*D***). ***B,*** Baseline-normalized motion index computed in 5 s contiguous time windows. ***C,*** Sleep (black segments, includes REM and NREM) and awake (white segments) periods computed based on the motion index and the theta/delta ratio. ***D,*** Percentage of time spent sleeping during the baseline (pre) and post-training (post) periods. ***E,*** Scatter plot of NREM versus awake non-normalized, average fEPSP slopes (Volts/s, with the sign reversed). Each data point represents a single electrode in panel ***A***. For a given electrode, the raw fEPSP slopes in multiple segments of NREM or awake state were collected together and then averaged. Mice with less than 5 min of NREM were excluded. Open circles represent the post-training period (n = 19 mice). Filled magenta circles represent the baseline period (n = 3 mice). ***F,*** Data from panel ***E*** are plotted as the ratio of the NREM period fEPSP slopes over the awake period slopes. Mean and error bars are computed with post-training data only; *** $p < 0.001$, for the post-training period, slope ratio is significantly different from 1; #, indicates no statistics were done on the pre-conditioning sleep due to the small sample size. ***G,*** Average normalized fEPSP slopes from the most potentiated electrodes (n = 24 mice, 1 electrode/mouse) after removing the fEPSP slope data corresponding to sleep segments shown in ***C***. ** $p < 0.01$, significant increase in fEPSP slopes in the post-training period relative to baseline. ***H***, as in ***G*** except that least potentiated electrodes (n = 18 mice, 1 electrode/mouse) were used. Error bars: SEM. Colormap in ***A*** & ***B*** clipped at 99th percentile.

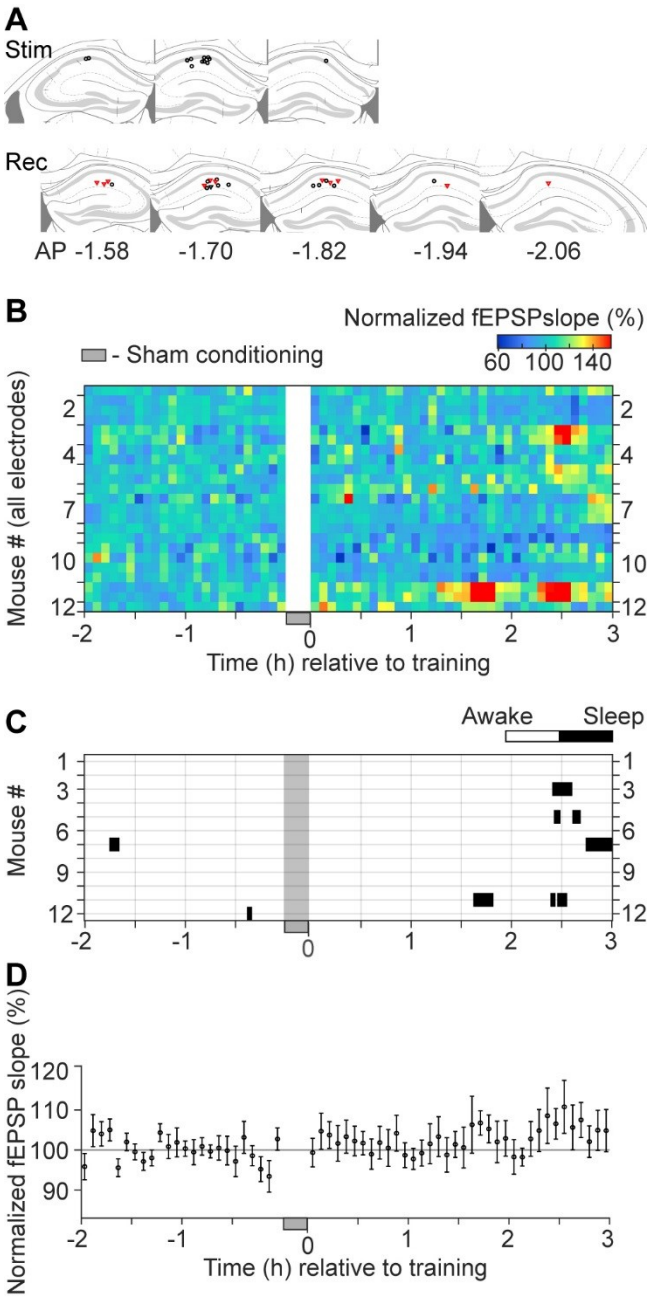

Figure 5. In vivo synaptic strength modifications associated with sham-conditioning. ***A,*** Locations of the tips of the stimulating (stim) and recording (rec) electrodes mapped onto a standard mouse atlas (Franklin and Paxinos, 2008). Red triangles indicate the single most potentiated electrode out of each mouse; those electrodes were used to indicate the largest measureable potentiation and were used in panel ***D.*** ***B***, Heat map of fEPSP slopes normalized to the baseline. Each row shows data from an electrode. Rows between adjacent ticks on the vertical axis indicate multiple electrodes recorded from a given mouse. The training period is marked by a gray box near time zero on the x-axis. ***C***, Sleep (black segments) and awake (white segments) periods were computed based on the motion index and the theta/delta ratio. ***D,*** Average normalized fEPSP slopes from the most potentiated electrodes (n = 12 mice, 1 electrode/mouse, locations marked by red triangles in ***A***) after removing fEPSP slope data corresponding to sleep segments shown in ***C.*** Error bars: SEM. Colormap in ***B*** clipped at 99th percentile.

Supplemental materials

Computing spectrogram based on Morlet wavelet transform

For the spectrogram in Figure 3B, we computed a continuous wavelet transform in MATLAB using complex Morlet wavelets ($\psi(t)$) defined by the following equation:

$$\psi(t) = \frac{1}{\sqrt{\pi F_b}}\, e^{-\frac{t^2}{F_b}}\, e^{i2\pi F_c t} \qquad 2$$

In this equation, t is time, F_c is the center frequency of the wavelet, and F_b controls how fast the wavelet decays in the time domain. The energy spread of the wavelet in the frequency domain is a Gaussian and the parameter F_b is inversely related to the variance (σ_f^2) of this Gaussian by the following relationship:

$$F_b = \frac{1}{2(\pi\sigma_f)^2} \qquad 3$$

To compute the spectrogram in Figure 3B, we created a series of 30 wavelets (half width of 2.5 s) by varying σ_f (0.125 to 2.5Hz) and F_c(1 to 30Hz) both on a logarithmic (10 based) scale. Each wavelet was then normalized to have unit norm. The raw data (sampled at 32 KHz) was first down-sampled to 320 Hz, and its wavelet transform was then computed in 30s-long contiguous data segments with a 2s buffer at either end of each segment. The resulting spectrogram was z-scored across the frequencies at each time point.

Linear mixed model analysis (LMM)

We describe the LMM using an example with 120 fEPSP slope measurements during baseline and 180 in post-learning period. The subjects (mice) are treated as random effects and time points of different segments (see below) are treated as fixed effects. The fEPSP slope (S_{tj}) of an electrode from a mouse (j) at a given time point (t) is modeled as follows:

$$S_{tj} = \beta_{0j} + \beta_1 X_{1tj} + \beta_2 X_{2tj} + \beta_3 X_{3tj} + \epsilon_{tj} \qquad 4$$

Where, β_0 denotes subject-specific intercept and ϵ_{tj} denotes error associated with slope S_{tj}.
Time (in minutes) since the beginning of the experiment is denoted by X_{1tj} where

$$X_{1tj} = [1, 2, 3, \dots, 300]$$

At each time point, the pre- and post-learning conditions are coded as 0's and 1's respectively (dummy coding) by X_{2tj} where

$$X_{2tj} = [0, 0, 0, \dots, 0_{180}, 1, 1, 1, \dots, 1_{300}]$$

Time since "interruption" (fear conditioning) is denoted by X_{3tj} where

$$X_{3tj} = [0, 0, 0, \dots, 0_{180}, 1, 2, 3, \dots, 180]$$

β_0, and β_1 can be interpreted by applying the values of X_1, X_2 and X_3 in Eq.4.
For the baseline period ($t \leq 120$), we obtain

$$S_{tj} = \beta_{0j} + \beta_1 X_{1tj}$$

Hence, a non-significant β_1 parameter would indicate that there is no significant drift in the baseline. Similarly, for the post-learning period ($t > 120$)

$$S_{tj} = (\beta_{0j} + \beta_2) + \beta_1 X_{1tj} + \beta_3 X_{3tj}$$

Hence, a significant β_2 parameter would indicate that there is significant shift in the level of post-learning data points relative to baseline. A non-significant β_3 would suggest that the post-learning trend is not significantly different from that of baseline. That is, the interruption did not significantly alter the ongoing trend (if any) in the baseline.

For directly comparing the learning effect in the fear-conditioned group against that of the sham-conditioned group, the model complexity was reduced by first removing components containing gain parameters - $\beta_1 X_1$ and $\beta_3 X_3$ (see Eq. 4) and adding a component $\beta_4 X_4$ where X_4 codes data points from shocked and control (sham) groups as 1's and 0's respectively. In addition, a term for interaction between pre-post and shocked-sham conditions - $\beta_5(X_{2tj}X_{4tj})$ - was included.

$$S_{tj} = \beta_{0j} + \beta_2 X_{2tj} + \beta_4 X_{4tj} + \beta_5(X_{2tj}X_{4tj}) + \epsilon_{tj}$$

A significant β_5 parameter would indicate that the change in the fEPSP slopes in the post-conditioning period relative to baseline, depends on the shocked-sham condition.